Atomic and electronic structure of decagonal Al-Pd-Mn alloys and approximant phases

M. Krajčí* and J. Hafner
Institut für Theoretische Physik, Technische Universität Wien, Wiedner Hauptstraße 8-10/136, A-1040 Wien, Austria

M. Mihalkovič
Institute of Physics, Slovak Academy of Sciences, Dúbravská cesta 9, SK 84228 Bratislava, Slovakia
(Received 5 June 1996)

The electronic structure of the decagonal phase $Al_{70}Pd_{13}Mn_{17}$ and related crystalline phases has been calculated using the self-consistent tight-binding linear-muffin-tin-orbital technique. The electronic densities of states and the spectral functions have been calculated via the real-space recursion technique. The structural models are based on the decagon-pentagon-hexagon tiling. Chemical short-range order is optimized using the information about the local densities of states. The pentagonal columnar clusters (identified by Hiraga *et al.*) exhibit structural stability and play the role of a characteristic structural unit of all the discussed phases. Formation of a pseudogap in the Al-sp band is observed and its origin and role in the stabilization of the decagonal phase is discussed. [S0163-1829(97)04201-X]

I. INTRODUCTION

Quasicrystals differ from ordinary crystals by possessing quasiperiodic rather than periodic translational order and a noncrystallographic orientational order.[1] Icosahedral (i) quasicrystals are quasiperiodic in three dimensions. Decagonal (d) quasicrystals have a crystalline axis perpendicular to a quasiperiodic plane with tenfold symmetry. Soon after the discovery of quasicrystals it was proposed that electronic effects play an important role in understanding their stability.[2,3] It has been proposed that diffraction by icosahedral Bragg planes leads to the formation of a structure-induced minimum in the density of states (pseudogap) at the Fermi level promoting a lowering of the structural energy of the icosahedral phase, as proposed by Hume-Rothery[4] and Jones[5] for certain classes of crystalline alloys. *Ab initio* calculations of the electronic structure of icosahedral quasicrystals[6–11,15] have shown that although a pseudogap at the Fermi level is a *generic* property of the icosahedral phase, in most cases it is not a *specific* property associated with quasicrystallinity. Pseudogaps have also been found in crystalline approximants and even in glassy and liquid phases of similar composition.[9,10] For the Al–transition-metal alloys it has been suggested very early[12,13] that a pseudogap can also originate from the antiresonance effect created by the strong hybridization of the transition-metal d band with the s,p band of Al. It has also been emphasized that the proximity of the resonance energy and of a quasi-Brillouin-zone-induced gap can lead to a special enforcement of the pseudogap.[12–14] However, in each case one has to examine very carefully the relative importance of structural and sp-d-hybridization effects in the formation of the pseudogap.[14,15]

Much less is known on the electronic structure of the decagonal alloys. While *ab initio* calculations for the lowest-order approximants to decagonal AlCuCo alloys[16] (based on the Burkov model[17] for the atomic structure) predict a pronounced pseudogap at the Fermi level, this is contradicted by photoelectron spectroscopy[18] and calculations on higher-order approximants to a variant of the same structural model.[19] The two theoretical results must not necessarily be contradictory, because the lowest and higher approximants show appreciable differences in their chemical compositions. In addition, the last-mentioned calculations as well as studies of the electronic structure of clusters existing in the Burkov model[20] have demonstrated that the existence/nonexistence of a pseudogap depends critically on the relative abundance and the local chemical order of the transition-metal atoms. In this context it seems also to be fair to say that the Burkov model in its original form is probably not an entirely satisfactory description of the decagonal structure.

In the present work we concentrate on the theoretical prediction of the electronic spectrum of decagonal AlPdMn.[21–23] Our description of the atomic structure is based on the tiling of the quasiperiodic planes with decagons (D), pentagonal stars (P), and squashed hexagons (H) (DPH tiling) proposed by Hiraga and Sun.[22] The electronic spectrum of the decagonal approximants and related crystalline phases ranging from the R phase and T phase with 156 atoms in the cell up to the τ^3-T phase with 2771 atoms has been calculated using the self-consistent tight-binding–linear-muffin-tin-orbital[24,25] (TB-LMTO) technique. We calculate the total and local densities of states and the total and partial Bloch-spectral functions. The chemical short-range order of the structural models is optimized on the basis of the electronic-structure calculations. Formation of a pseudogap is observed in the Al-sp band, its origin and role in stabilization of the decagonal phase is discussed.

II. QUASIPERIODIC PHASES IN THE AL-PD-MN SYSTEM

The success in the preparation of the large thermodynamically stable quasicrystalline grains of the icosahedral AlPdMn phase initialized a boom of experimental and theoretical investigations. The structure and the properties of these materials are today well understood.[15] The preparation of large grains of the decagonal AlPdMn phase discovered

by Beeli *et al.*[21] has proved to be more difficult. The detailed metallurgical investigation of the ternary Al-Pd-Mn phase diagram in the region of quasicrystalline phases performed by Audier *et al.*[23] and later by Gödecke *et al.*[26] has clarified that around the chemical composition $Al_{70}Pd_{13}Mn_{17}$ various crystalline phases coexist with the decagonal phase. The high-resolution electron microscopy (HREM) images helped to reveal[27] a close structural relationship between the decagonal phase and crystalline Al_3Mn (i.e., Taylor's phase[28] or T phase). Hiraga *et al.*[27] have performed a crystallographic study of Al_3Mn in order to propose an atomic arrangement for the decagonal structure. Two other crystalline phases were identified in the phase diagram: one is related to the Robinson phase $Al_{60}Ni_4Mn_{11}$[29,30] (this phase is heretofore referred to as R phase) and the other has two of its cell parameters τ^2 times larger [τ is the golden mean $\tau=(1+\sqrt{5})/2$] than those of the R phase (we refer to this phase as the τ^2-R phase; in Ref. 31 it is called the D_H phase).

On the Pd-rich side of the phase diagram a stable *i* phase with the approximate composition $Al_{70}Pd_{22}Mn_8$ is observed. The icosahedral phase has a meta(?)stable (2/1)-approximant phase[32] with composition $Al_{70}Pd_{26}Mn_4$ and is related to the ξ phase described by Audier *et al.*[23] The icosahedral phase also has a remarkable structural relationship to the crystalline Al_6Mn phase.[33]

It has to be pointed out that although the HREM technique has led to the identification of the decagonal phase and of a number of related crystalline phases, this technique does not yield precise information about the positions/chemistry of all the atoms constituting the structure. On the other hand, the single-crystal diffraction refinements performed by Steurer *et al.*[34] and Yamamoto *et al.*[35] helped to clarify some details of the structure but even in this case averaging over (phason) disorder present in the structure puts rather severe limitations on the accessible resolution.

A. Structural relationships

The structure of the Al-Pd-Mn decagonal quasicrystal and its related crystalline phases with 12.5 Å periodicity can be interpreted according to Hiraga and Sun[22] as different packings of a single pentagonal columnar cluster. The clusters can be represented by pentagons in the projection onto the plane perpendicular to the axis of the columns and whenever they share an edge, the two corresponding clusters are related through the two-fold screw symmetry operation. This packing rule can be depicted by assigning pentagons two colors as in Fig. 1. Joining the centers of pentagons perpendicularly to their edges forms a tiling that offers a unified description of the decagonal phase and its related crystalline ''approximants.''

While both R- and T- phases geometries become two different tilings of a single hexagonal supercell H [Figs. 1(a,b)], the HREM images[21,22,36] reveal that in decagonal phase three other supercells occur: a pentagonal star (P), a decagon (D), and an ''octagonal ship'' (O). While the D, P, and H units are typically found in the ''bulk'' regions of the images and are stable upon temperature treatment (annealing), the O unit is typically found in boundary regions and is found unstable upon annealing.[22,37] The mutual relationship of the D, P and H tiles and the small pentagons representing pentagonal clusters is obvious from Figs. 1(c,d,e). In the following we will term the tiling of these three supercells ''DPH'' tiling.

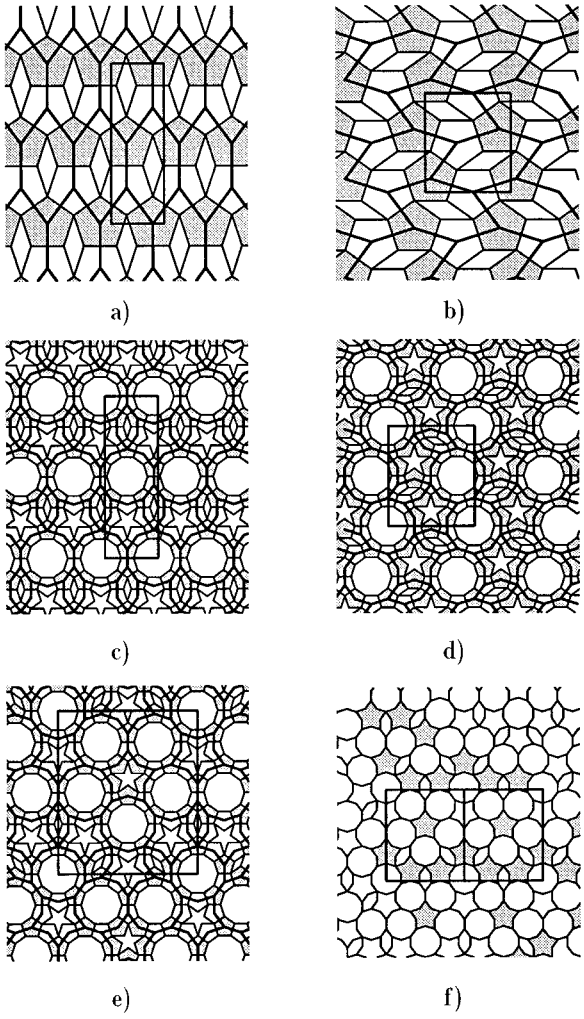

FIG. 1. Structural models of the decagonal phase and its approximants is based on a tiling of decagons (D), pentagonal stars (P), and a squashed hexagons (H). The R phase (a) and T phase (b) are different tilings of H tiles. An elementary cell of both τ^2-R phase (c) and τ^2-T phase (d) consists of 2 D tiles, 2 P tiles, and 2 H tiles. The next larger approximant to the decagonal phase is the τ^3-T phase phase (e) consists of 6 D, 5P, and 3H tiles per elementary cell. (f) represents the DPH tiling taken from an experimental HREM image (Fig. 2 in Ref. 34) containing two unit cells of the τ^3-T approximant to the decagonal phase. Thick lines show DPH tiling, thinner lines show the decomposition of DPH tiling to Hiraga's pentagonal columnar clusters. The rectangles indicate the unit cells. Coloring of pentagons represents twofold screw symmetrical relationship between the columnar clusters decorating pairs of edge-sharing pentagons.

Along the direction of the (pseudo)decagonal symmetry axis, the R and T phases can be desribed as stackings of two types of atomic layers:[36] *F* (for flat layer) and *P* (for puckered layer). The stacking sequence of layers within the unit cell is *PFPpfp* where the layers *F* and *f* or *P* and *p* are planes related by inversion symmetry operation. In the perfect quasiperiodic decagonal phase without phason strains the *PFP* and *pfp* sandwiches would be related by tenfold screw symmetry operation. The presence of phason fluctua-

tions or of a constant background phason strain (periodic approximants) breaks this symmetry and it is necessary to redefine the layer relationships *locally* for each type of supercell constituting the tiling (see next subsection).

While the ''ideal'' quasiperiodic tiling by all four D, P, H and O units can be described as a projection of compact atomic surfaces embedded in five-dimensional (5D) space (it is a decoration of the binary Penrose tiling), the true quasiperiodic DPH tiling has a nontrivial 5D representation with fractal atomic surfaces[38] and it is closely related to the geometry of the maximal density disk packing with decagonal symmetry.[39] The approximants used in this study are based on the DPH tiling.

B. Structural models

In this section we at first briefly introduce the tiling-decoration approach to the quasicrystal structure modeling that allows efficient parametrization of the periodic and quasiperiodic structures with arbitrary phason strains by few parameters. The parameters—coordinates and chemistry of the ''topologically inequivalent sites''—are then the input for self-consistent electronic structure calculations. Our model of the *d*-AlPdMn phase and its periodic approximants is formulated as a decoration rule for the DPH tiling; we describe the decoration rule and characterize the five approximants studied here.

1. Tiling-decoration model

The quasiperiodic or periodic tiling-decoration model is obtained by assigning to the tiling objects (vertices, edges, faces . . .) identical atomic motifs. This procedure reduces the problem of identifying an infinite number of inequivalent atomic positions in the quasicrystal to that of determining a finite set of sites assigned to the tiling objects. The number of topologically inequivalent sites is further reduced if we demand that the atomic motif has to have the same point symmetry as the tiling object to which it is ''bound.'' For example, all pentagonal rings of atoms bound to the vertices of the tiling are represented by a single topological site with pentagonal symmetry.

An important aspect of this concept is that it offers control over the *accuracy* within which the atoms merged into single topological class are equivalent (note that in quasicrystal, *none* of the atomic environments are strictly equivalent). For example, if it turned out that the atomic positions in the pentagonal rings bound to the tiling vertices should be occupied by more than one species, they could be ''rebound'' to other tiling objects with lower point symmetry, thus splitting the single topological class into more classes, and effectively increasing the cutoff radius within which each atomic position belonging to a topological class is strictly equivalent.

In the following, we will loosely refer to our atomic model of *d*-AlPdMn and its approximants in terms of decoration of the D, P, and H tiles. However, the actual ''binding'' we used employed five flavors of vertices, edges, and the P and H tiles were broken into triangles of two flavors and rectangles, yielding 31 topological sites for general DPH tiling model (see Fig. 2).

Our decoration rule for the DPH tiling follows closely the proposal of Hiraga and Sun.[22] At each DPH tiling vertex we place the pentagonal cluster: Figs. 1(c,d,e) illustrate that the ambiguous regions that remain are near the centers of the D and P supercells. The same figure reveals an interesting consequence of the twofold screw relationship between the edge-sharing pentagonal motifs: while the D tile (as well as H tile) appears in a *single* flavor, there are two *distinct* flavors of the P tile: its central part decoration is constrained by either five white or dark pentagons. Thus, a generalization of the R- and T-phase model requires: (i) guessing the PFP motif for the central region of the D tile; the D(pfp) motif is related to it by the tenfold screw symmetry operation, (ii) guessing *both* PFP and pfp motifs for the central region of the P tile; these are two *distinct* motifs. The whole structure could be then interpreted as a packing of two robust columnar motifs associated with the D and P tiles; the D columns with tenfold screw symmetry are mutually related by pure translations in the quasiperiodic plane, while the P columns with only pentagonal symmetry split into two flavors that are mutually related by tenfold screw symmetry (plus translation in the quasiperiodic plane) operation.

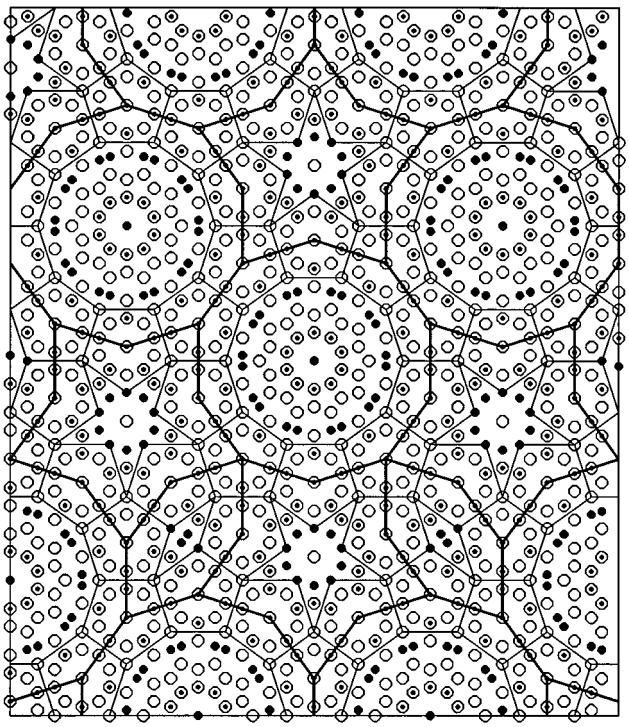

FIG. 2. Structural model for the τ^3-T approximant to the decagonal AlPdMn phase: Projection of the positions of atoms of an unit cell on a plane perpendicular to the periodic axis. Open circles denote Al atoms, large closed circles denote Pd atoms, small closed circles denote Mn atoms. Thick lines show DPH tiling, thinner lines show decomposition of DPH tiling to Hiraga's pentagonal columnar clusters.

As a D(PFP) and P(PFP) and P(pfp) motifs we again adopt the proposal of Hiraga and Sun (which is in turn inspired by—but not identical to) the proposal of Steurer *et al.* based on single-crystal refinement.[34] Topologically, our modification of Hiraga's model consists in avoiding some pairs of atoms too close to each other: all of these conflicts can be resolved by splitting the puckered layers (P and p) into sublayers, truly reflecting the ''puckering.'' In our

TABLE I. Structural characteristics of our DPH-tiling *d*-AlPdMn model. Al, Pd, and Mn contents are given fractionally, the last two columns give frequency (relative to the P-tile frequency) and fractional volumes associated with each kind of tile at zero average phason strain (decagonal state).

	Atoms	Al	Pd	Mn	ρ [at. Å^{-3}]	f	V_f
D	282	0.716	0.149	0.135	0.0677	1.236	0.618
P	169	0.686	0.118	0.196	0.0656	1	0.309
H	78	0.692	0.103	0.205	0.0677	0.527	0.073

model, each puckered layer is splitted into four sublayers.

The interesting feature of our model is that we attempted to optimize the chemical short-range order on the basis of the local electronic-structure calculations. The result is summarized in Tables I and II where we display the chemical composition and atomic densities of the D, P, and H tiles themselves and in approximant phases. The optimization is discussed in detail in Secs. IV B and IV E. In Fig. 8 we show the precise placements of the 31 topological sites and their chemical identity.

2. Approximants

As we already noted the quasiperiodic DPH tiling is defined by acceptance domains with fractal boundaries and therefore the construction of periodic approximants cannot be approached within the hyperspace scheme. Finite-size approximants to the quasiperiodic DPH tiling can be obtained by the Monte Carlo technique as described in Ref. 39, or one has to follow the τ^6-inflation procedure of Cockayne,[38] or the small approximants used here can be simply constructed by hand. Our approximant with the biggest unit cell was inspired directly by experimental HREM image [Figs. 1(e,f)].

The sequence of five approximant models we study here includes: T and R phases containing only H tiles, τ^2-R and τ^2-T phases being the smallest possible approximants containing all D, P, and H tiles, and a model of a τ^3-T phase with 2771 atoms in the unit cell standing as a fairly good approximation to the decagonal phase.

To retain a consistency among the chosen set of models we had to adopt certain idealizations. Althought the atomic coordinates in the unit cells of R and T phases are available from diffraction refinements, we preferred to use uniformly for all models the ''idealized'' coordinates which are in the projection onto the quasiperiodic plane integer linear combinations of the appropriate pentagonal basis vectors. Another idealization consisted of replacing fractionally occupied sites observed in the T phase by fully occupied sites; the chemical order in both T and R phases has been adjusted to facilitate the comparison of the total electronic energies. Thirdly, all lattice parameters are set to values corresponding to a center-to-center pentagon spacing of $d_q=4.8$ Å, and the periodic repeat distance perpendicular to the (pseudo)decagonal plane to $c=12.43$ Å according to Audier *et al.*[23]

The model of the T phase is based on structural data obtained from the single-crystal x-ray refinement of Hiraga *et al.*[27] The chemical composition of their sample was close to Al_3Mn. A detailed structural information was obtained from a combination of Patterson analysis and HREM. The orthorhombic unit cell with lattice parameters $a=14.8$ Å, $b=12.59$ Å, $c=12.42$ Å contains 156 atoms. The space group is *Pnma* (No. 62). Chemical order has been slightly idealized: the positions denoted as Mn_8 and Mn_9 are occupied in the original model with 50 and 40 % probability, respectively, by Al atoms are now occupied by Al atoms only. All other fractional occupancies were replaced by the majority atom. This replacement preserves the columnar pentagonal clusters of Al-Mn atoms constituting the backbone of the DPH tiling geometry. The modification slightly decreases the content of Mn atoms in the model to $Al_{79.5}Mn_{20.5}$. As already noted although the detailed information about the positions of atoms is available from the x-ray refinement, we preferred a model with idealized positions of atoms. The idealized model is thus consistent with other models of larger approximants to decagonal phase described below. Figure 1(a) shows the projection of the unit cell on the plane perpendicular to the ''decagonal'' *c* axis. In our model of idealized T phase we distinguish 15 topologically different sites (see Table II).

The structure of the complex orthorhombic phase $Al_{60}Ni_4Mn_{11}$ was crystallographically resolved several decades ago by Robinson.[29,30] The unit cell ($a=7.75$ Å, $b=7.75$ Å, $c=12.5$ Å) has orthorhombic symmetry, space group *Cmcm* (No. 63) and contains 156 atoms. The Ni atoms were replaced by Mn and in order to preserve the structure of the pentagonal clusters existing on the T phase, the Al_9 atom was replaced by Mn. With this modification, the composition of the R phase is identical to that of the T phase. The schematic representation of the T- and R-phase models in terms of colored pentagonal tiling (thin lines) and H tiling (thick lines) is shown in Figs. 1(a,b).

The next smallest possible approximants contain already all three kinds of D, P, and H tiles. In analogy to the T- and R-phase tilings, the two basic variants are possible: ''τ^2-T'' and ''τ^2-R'' [Figs. 1(c,d)]. While the τ^2-T structure is a hypothetical phase, the τ^2-R phase has been observed experimentally. The intricacies of the equilibrium phase diagram leading to the formation of decagonal or τ^2-R phase are described in Refs. 26, 36, and 40. A distinct structural feature of both DPH tilings is that each contains a *single* kind of P tiles.

Interestingly, both τ^2-T and τ^2-R DPH tilings may occur in variants, even if the network of D tiles is fixed. This is due to the fact that the P and H tiles form infinite open chains,

TABLE II. Structural data of the crystalline R and T phases and *d*-AlPdMn approximants. Lattice parameters *a* and *b* are given in the units of the pentagon edges $d_q=4.8$ Å, (see Fig. 1), $\eta=(\tau+2)^{1/2}$. *c* parameter (repeat along periodic axis) is 12.43 Å. Last column reports the numbers of topologically inequivalent sites in each model.

	D	P	H	Atoms	*a*	*b*	Topo
T phase			2	156	τ^2	$\tau\eta$	15
R phase			2	156	τ	$\tau^2\eta$	15
τ^2-T	2	2	2	1058	τ^4	$\tau^3\eta$	31
τ^2-R	2	2	2	1058	τ^3	$\tau^4\eta$	31
τ^3-T	6	5	3	2771	τ^5	$\tau^4\eta$	31

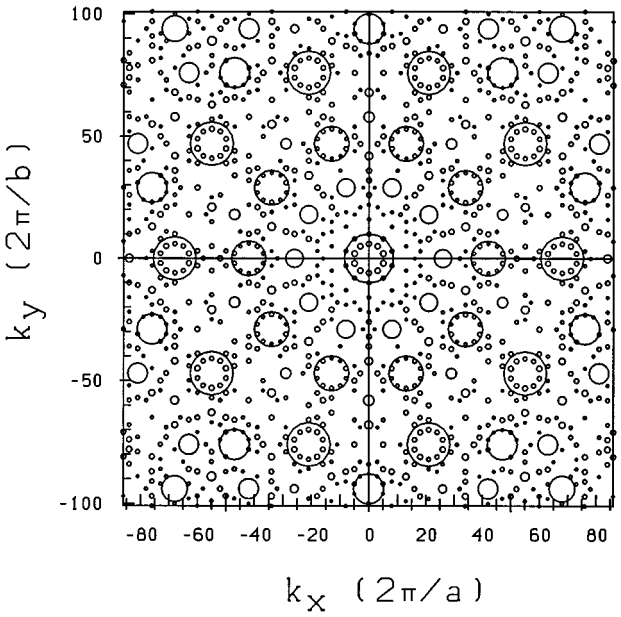

FIG. 3. Neutron-diffraction pattern of the τ^3-T approximant to the decagonal AlPdMn phase in a plane perpendicular to the periodic axis. Areas of the circles are proportional to the intensity of the diffraction peaks.

contrary to the decagonal state when each such chain is finite and surrounded by D tiles, which is a consequence of the binary character of the DPH tiling. The open chains may be flipped in such a way that (roughly speaking) the positions of P and H tiles are altered (and the P tile changes flavor). The variants correspond to distinct atomic structures. In this paper we consider only one variant of each of the two phases, shown in Fig. 1.

Finally, the approximant with the biggest unit cell (we denote it τ^3-T following the nomenclature based on lattice parameters) we considered here is shown in Fig. 1(e). The relative frequencies of the D, P, and H tiles are 6:5:3, very close to the relative frequencies in the true decagonal state, equal to 1.236:1:0.527. (Note that the relative tile frequencies are only a function of a constant background phason strain; therefore they apply to both perfectly quasiperiodic or random decagonal DPH tilings in the case of zero background phason strain). Our choice of this approximant was guided by several criteria: we wanted to test a model of a size approaching the limitations of our computer resources and—last but not least—a few unit cells of this approximant can be clearly identified in the experimental HREM image[41] of the decagonal phase. Figure 3 shows the calculated neutron diffraction pattern for the τ^3-T phase in a plane perpendicular to the periodic axis. Note the almost perfect tenfold symmetry of the pattern and the quasiperiodic sequence of intense diffraction peaks along the twofold axes. The numbers of atoms per unit cells, their tile content, lattice parameters and the number of inequivalent topological sites for each approximant can be found in Table II.

III. SELF-CONSISTENT REAL-SPACE TIGHT-BINDING LMTO METHOD

The smallest approximant to the decagonal quasicrystal containing the characteristic structural feature of the decagonal quasicrystals—the decagonal cluster (D tile)—involves more than 1000 atoms in the unit cell. As the quasicrystals are typically multicomponent systems, a self-consistent calculation of the electronic structure is necessary. This is particularly important in the case of the AlPdMn system containing two different transition metals where the interaction of the transition-metal atoms leads to significant changes of the position and width of the *d* bands of the two transition metals[42–44] during the self-consistent iterations. Fortunately quasicrystals are ordered systems and the number of locally topologically nonequivalent sites is limited (within a finite cutoff radius, see Sec. II B 1), in our model we consider around 30 topologically different sites.

For such systems we used with success the self-consistent real-space tight-binding LMTO method. The method is based on the tight-binding LMTO formalism.[24] The Hamiltonian is transformed from the standard LMTO basis to the most localized tight-binding basis. Some details of the application of the TB-LMTO formalism to quasicrystalline approximants are given also in our previous paper.[9] The LMTO structure constants are calculated for each atomic site, including all neighbors within a sphere containing 20 atoms on average. For the construction of the Hamiltonian we used as the initial potential parameters values tabulated for the pure metals. The two-center TB Hamiltonian in the Löwdin orthonormal representation is determined in terms of an expansion in powers of the nonorthogonal TB Hamiltonian in the screened, most localized basis and the overlap matrix. This expansion is truncated at the second-order term. The local densities of states (DOS) of all topologically nonequivalent atoms are calculated using the recursion method.[45] The local DOS was obtained by summation over contributions from *s*, *p*, and *d* orbitals. We used typically 20 recursion levels and the Lucchini-Nex terminator.[46] Good results were obtained also with the Gaussian[47] terminator. The valence charge density of an atom is reconstructed from the moments of the local DOS. The core charge density is obtained from relativistic self-consistent calculation of free atoms. The Madelung constants are calculated by the Ewald summation technique. The Kohn-Sham potential is constructed within the local-density approximation. For the exchange-correlation potential the Barth-Hedin formula is used.[48]

We performed the calculation in real space, i.e., only for the Γ point in the Brillouin zone. As this is not satisfactory enough for T and R phases with a relatively small unit cell (156 atoms), we constructed a supercell containing eight elementary cells, i.e., 1248 atoms. Such a multiplication of the elementary cell does not increase the number of topologically nonequivalent sites and the computer time scales linearly with the total number of atoms in the supercell. The energy resolution depends on the number of recursion levels, which is, however, limited by the size of the model. At the end of the self-consistent iterations we increased the energy resolution by increasing the number of the recursion levels to 80. We increased correspondingly the size of the model by multiplication of the elementary unit cell to more than 8000 atoms.

The integrated total density of states was calculated by summation over the local DOS. We calculated the total DOS also by the recursion technique utilizing randomly phased vectors as the initial vectors. We got almost the same results

for both approaches. This proves that the choice of the restricted number of the nonequivalent sites in the models with a large unit cell is sufficiently representative.

The information about the local DOS allows to evaluate the local contributions to the band energy from the individual sites. We used this information for optimization of the chemical short-range order in our models.

In addition to the local and total densities of states we calculated also the Bloch-spectral functions for selected directions in k space. The Bloch-spectral function can be conveniently calculated by the recursion method using a plane wave as an initial state. Details are given in our previous papers.[49]

IV. ELECTRONIC STRUCTURE

A. Electronic structure of the T and R phase

Figure 4(b) shows the total and partial Al and Mn densities of states for the model of the T phase. The T-phase model with the composition $Al_{79.5}Mn_{20.5}$ shows an Al band with a width W = 10.2 eV that is slightly lower than that in pure crystalline Al (W = 11.4 eV). The structure of the Al band is essentially free-electron-like (parabolic) over a wide energy range and shows a broad and deep depression around the Fermi level. The minimum of this pseudogap is about 0.7 eV above the Fermi level. The Mn band has its maximum about 1.3 eV below the Fermi energy. Because of the relatively high Mn concentration and the chemical order the Mn-d band has lost the character of an impurity band and the bonding–antibonding splitting that characterizes the transition-metal d bands should be considered in the formation of shape of the band. The Fermi level is located near a small local minimum of the total DOS created presumably by the hybridization of Al-sp band with the Mn-d band. The DOS at E_F is relatively high.

Figure 4(a) shows the total and partial Al and Mn densities of states for the R phase. Our model for the R phase has the same composition ($Al_{79.5}Mn_{20.5}$) as the T phase and shows an Al band with a width W of 10.2 eV, the same as in the T phase. Although the structure of the Al band is essentially free-electron-like, it is again dominated by a deep pseudogap around the Fermi level. The pseudogap is more structured than in the case of T phase and exhibits a double well shape. The local subminima of the double-well are separated 1.7 eV. The Fermi level is located between them. The Mn band has its maximum similarly as for the T phase about 1.2 eV below the Fermi energy. The Mn band has in its upper part again a clearly resolved shoulder. The Fermi level is located near a small local minimum of the total DOS created by the coincidence of the shoulder of the Mn-d band and the first subminimum in the Al band. A similar coincidence of the second subminimum in the Al band with the next local minimum in the Mn band creates a deep pseudogap in the total DOS at 1 eV above the Fermi level. The upper part of the Mn band fills the pseudogap in the Al band and consequently the DOS at E_F is again relatively high. The coincidence of the local minima in Al-sp band and Mn-d band indicate that they may originate from the sp-d hybridization. It is remarkable that a similar split double-minima structure of the DOS has been observed also for the 1/1 approximant to icosahedral $Al_{70}Pd_{15}Mn_{15}$; see Fig. 4(c).

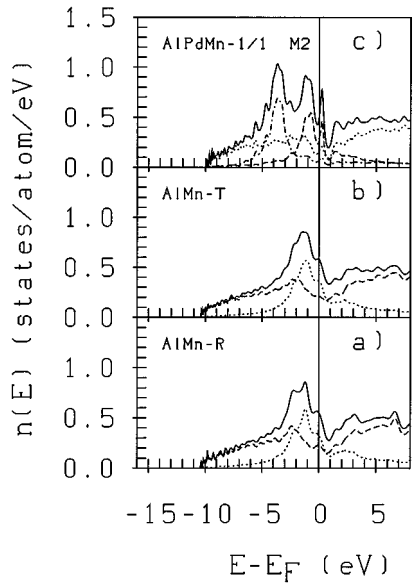

FIG. 4. Total and partial electronic densities of states: (a) AlMn-R phase, (b) AlMn-T phase, (c) 1/1-approximant to the icosahedral AlPdMn phase. Full line denotes total DOS, partial contributions to DOS: dashed line is for Al, dot-dashed line is for Pd, and the dotted line is for Mn.

Apparently the hybridization effect increases with increasing Mn content, which is much higher in the case of 1/1 approximant than in the icosahedral $Al_{71}Pd_{21}Mn_8$ phase (see Ref. 15).

As the difference in the structure of the T and R phases consists of a different arrangement of the same H tiles and hence the chemical composition of both models is the same, we can verify the relative stability of both phases by comparison of the band energies/atom. From the Andersen force theorem[50] it follows that under these circumstances the difference in the total energy is equal to the difference of the band energies. We found the band energy to be by ΔE_{band}=166 meV/atom lower for the R phase, indicating that the local DOS minimum in the Mn band promotes a certain amount of band-gap stabilization.

B. Optimization of the chemical short-range order

The unit cells of both τ^2-R and τ^2-T phases are already large enough to contain all substantial ingredients of the decagonal phase (they each contain one pair of D, P, and H tiles) and can be considered as the lowest-order approximant phases to the decagonal quasicrystal. As we have already noted the crystallographically solved T-phase structure determines the decoration of H units, but there is a certain ambiguity in the decoration of the P and the D units. The HREM observations provide information about the relative positions of the Al and transition-metal atoms but they cannot distinguish between different transition metals. Beeli and Horiuchi[31] attempted to solve this problem by comparison of the simulated HREM images with those experimentally observed. The single-crystal diffraction refinements[35,34] certainly obscure the short-range chemical order by averaging over phason disorder, and HREM refinement[31] alone cannot be considered as reliable and/or accurate; it is of interest to

test and complement this information by local electronic-structure calculations. We attempted to optimize the chemical short-range order on the basis of the local electronic-structure calculations.

Structural differences in the total energy are of the order 0.1 eV/atom and therefore high accuracy in the calculation of the electronic structure is necessary. The extremely accurate total-energy calculation of so complex quasicrystalline approximants exceeds the accuracy accessible by our method and for more accurate methods the size of the model (1058 atoms) is prohibitively large. Thus, we can only compare the structural energies at *fixed* stoichiometry and atomic density.

The number of different topological sites is 31. Each site is occupied by one atomic species. In our models we do not allow fractional occupancies. Each topological site has in the model a multiplicity which ranges from 4 (e.g., the site in the centers of the decagonal tiles) to 200 (Al atoms in the small pentagonal clusters). The optimization of the decoration is based on the analysis of the contributions from particular sites to the band energy of the model. By exchanging the occupations of a pair of sites we tried to lower the band energy. Stoichiometric constraints reduce the number of possible configurations. Although the band-energy information alone does not guarantee to obtain the configuration with the lowest total energy, it certainly excludes all energetically clearly unfavorable configurations. We considered also the size of atoms and the nearest-neighbor distances. We excluded also configurations which lead to unphysically large charge transfer among atoms.

First we optimized the decoration of the DPH tiling for the model of τ^2-T phase. We started from the decoration close to the proposal by Beeli and Horiuchi.[31] During the optimization we tested 14 different chemical variants. We observed that the small pentagonal Al-Mn clusters dominate the stability of the whole structure. The deep pseudogap in the Al band around the Fermi level contributes to the lowering of the band energy and the existence of the DOS minimum seems to be the most important stabilizing principle.

The decoration of the small pentagonal clusters almost completely determines the decoration of the H tiles and leaves only little ambiguity in the decoration of the P tiles. The decoration of the D tile is dominated by the central region which in the projection on the plane perpendicular to the decagonal axis appears as a decagonal ring (cf. Figs. 1 and 2). It is occupied mainly by transition metals (TM's), as is evident also from the HREM images. It is formed by a sequence of pentagonal TM and Al rings around the central TM atom. Contrary to the proposal of Beeli and Horiuchi[31] we found it energetically more favorable to place the Mn atoms on the pentagonal TM ring and a Pd or Al atom in the center, see Fig. 5(a). Putting a Mn atom in the center leads to a large charge transfer (1.2 electron) from the Mn atom with a very narrow *d* band positioned at the Fermi level to the surrounding atoms. The Pd atoms are located mostly inside the D tile between the central decagonal ring and the outer ring of the pentagonal Al-Mn clusters. Some Pd atoms are also located inside the P and H tiles. The optimized decoration of the tiles found for the τ^2-T phase was applied also to other approximants to the decagonal phase. The resulting decoration is shown in Figs. 2 and 8 and it is further discussed in Sec. IV E.

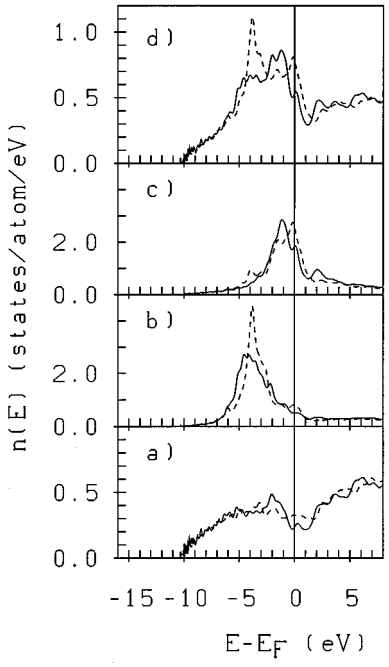

FIG. 5. Total and partial electronic densities of states for variants of the structure of the τ^2-R phase differing in chemical decoration: Dashed lines: Decoration close to the proposal by Beeli and Horiuchi (Ref. 21) with Al and Pd atoms in the decagonal ring of the central region Mn atom in the center of the D tile. Full lines: optimized decoration with the Pd atom in the central position, Al and Mn atoms alternating in the central decagonal ring. Other differences, see also, in Figs. 2 and 8. Partial contributions to DOS: (a) Al, (b) Pd, (c) Mn, (d) total DOS.

In Fig. 5 we show the total and partial electronic densities of states for variants of the structure of the τ^2-R phase differing in chemical decoration. Dashed lines corresponds to the initial decoration with Al and Pd atoms in the decagonal ring of the central region Mn atom in the center of the D tile. Full lines show the result for the optimized decoration. We can see the dramatic change of the total and partial densities of states of all components. In the optimized configuration the Al band exhibits a deeper pseudogap at the Fermi level and apparently promotes the stability of the system. Also the maximum and the center of gravity of the Mn band are clearly shifted to lower energies. We note that the composition of the initial decoration ($Al_{67.5}Pd_{15}Mn_{17.5}$) was somewhat different from that of the optimized model ($Al_{70.5}Pd_{13}Mn_{16.5}$).

C. Electronic structure of the approximant phases τ^2-R, τ^2-T, and τ^3-T

Figure 6 shows a comparison of the total and partial Al, Pd, and Mn densities of states for the models of the τ^2-R, τ^2-T, and τ^3-T phases. The overall electronic structure of all these approximants to the decagonal phase is rather similar. The bandwidth *W* of 10.0 eV is the same for all three systems and is almost the same as in the case of the T and R phases. The structure of the Al band is essentially free-

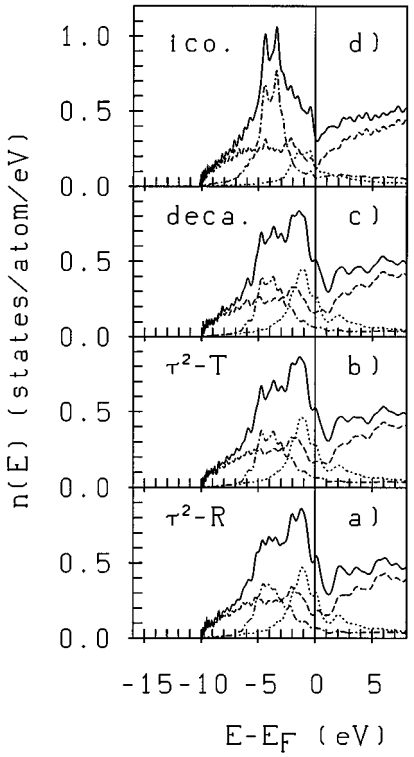

FIG. 6. Total and partial electronic densities of states of AlPdMn phases: (a) τ^2-R phase, (b) τ^2-T phase, (c) τ^3-T approximant to the decagonal phase, (d) 8/5-approximant to the icosahedral phase. Full line denotes total DOS, partial contributions to DOS: dashed line represents Al, dot-dashed line represents Pd, dotted line denotes Mn.

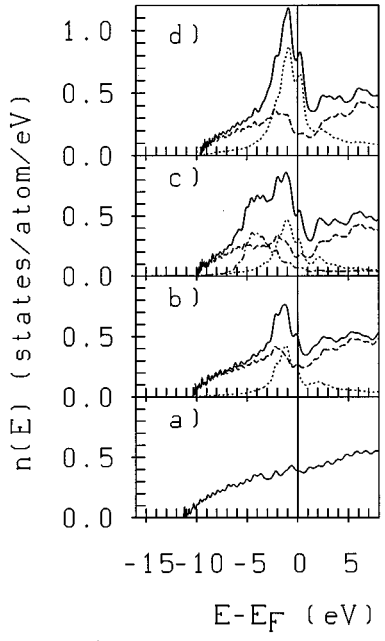

FIG. 7. Total and partial electronic densities of states of the τ^2-R AlPdMn phase. The chemical composition is varied in order to study the influence of different chemical decorations on the form of the DOS. (a) All sites are occupied by Al atoms, (b) only Pd atom are replaced by Al atoms, (c) original AlPdMn composition, (d) all transition-metal sites are occupied by Mn atoms. Full line denotes total DOS, partial contributions to DOS: dashed line denotes Al, dot-dashed line denotes Pd, dotted line denotes Mn.

electron like (parabolic) near the bottom and shows a broad depression around the Fermi level. Higher precision calculations for models with repeated elementary cells and more recursion levels reveal details of the form of the pseudogap in the Al band. It consists of two local minima separated by 1.2 eV. The first one is 0.2 eV below the Fermi level, while the second one is about 1 eV above E_F.

The broad Mn band is formed essentially by *d* states. It has its maximum about 1.2 eV below the Fermi level E_F. The decreasing part of the band is modulated by two local minima. The first one is located very close to the Fermi level (at -0.2 eV) and splits the band at a relatively high density of states. The second one lies deeper and is about 1 eV above the Fermi level. The position and distance of these local minima are almost the same as those in the Al band.

The coincidence of the position of the pair of local minima in the Al and Mn bands gives rise to the corresponding features in the total DOS. The Fermi level is located very close to the lower-energy local minimum and fits best to the minimum for τ^2-R phase. This could explain the larger stability of this phase in comparison to the τ^2-T phase. The latter has not been observed experimentally. The difference in the structure of both models consists in the different arrangement of the same DPH tiles and hence the chemical composition of both models is the same, we can again verify the relative stability of both phases by comparison of the band energies/atom. From the Andersen force theorem[50] it follows that under these circumstances the difference in the total energy is equal to the difference of the band energies. We found the band energy to be by $\Delta E_{\text{band}}=85$ meV/atom lower for the τ^2-R structure. The τ^3-T phase has a slightly different composition than the others and therefore a similar comparison is not meaningful. However, from the relative position of E_F with respect to the local minimum we can expect a lower stability than of the τ^2-R phase. This agrees with the experimental observation that the decagonal phase exists as a high-temperature phase where the stabilizing contribution from the entropy term can overrule the higher energetic stability of the crystalline τ^2-R phase.

We have already noted in Sec. IV A a similar splitting of Al and Mn bands can be recognized also in the electronic structure of the icosahedral AlPdMn phase; see Fig. 6(d). It is particularly well resolved in the case of the AlPdMn 1/1 approximant which has similar content of Mn atoms as the decagonal phase in Fig. 4(c). We assume that this splitting has origin in *sp-d* hybridization between Al-*sp* states and Mn-*d* states. This local subminima can contribute to the stability of the system, however, the main contribution to the stability comes from the deep depression in the Al band, which is created by the Hume-Rothery-like mechanism. This holds for the icosahedral and decagonal phase as well, but the effect of the *sp-d* hybridization is larger for the former one. It is also interesting to point out that, while for the decagonal phase and for the 1/1 approximant to *i*-AlPdMn the Fermi level is located near to or at the first local minimum, in the case of *i*-AlPdMn the Fermi level is located at the second minimum.

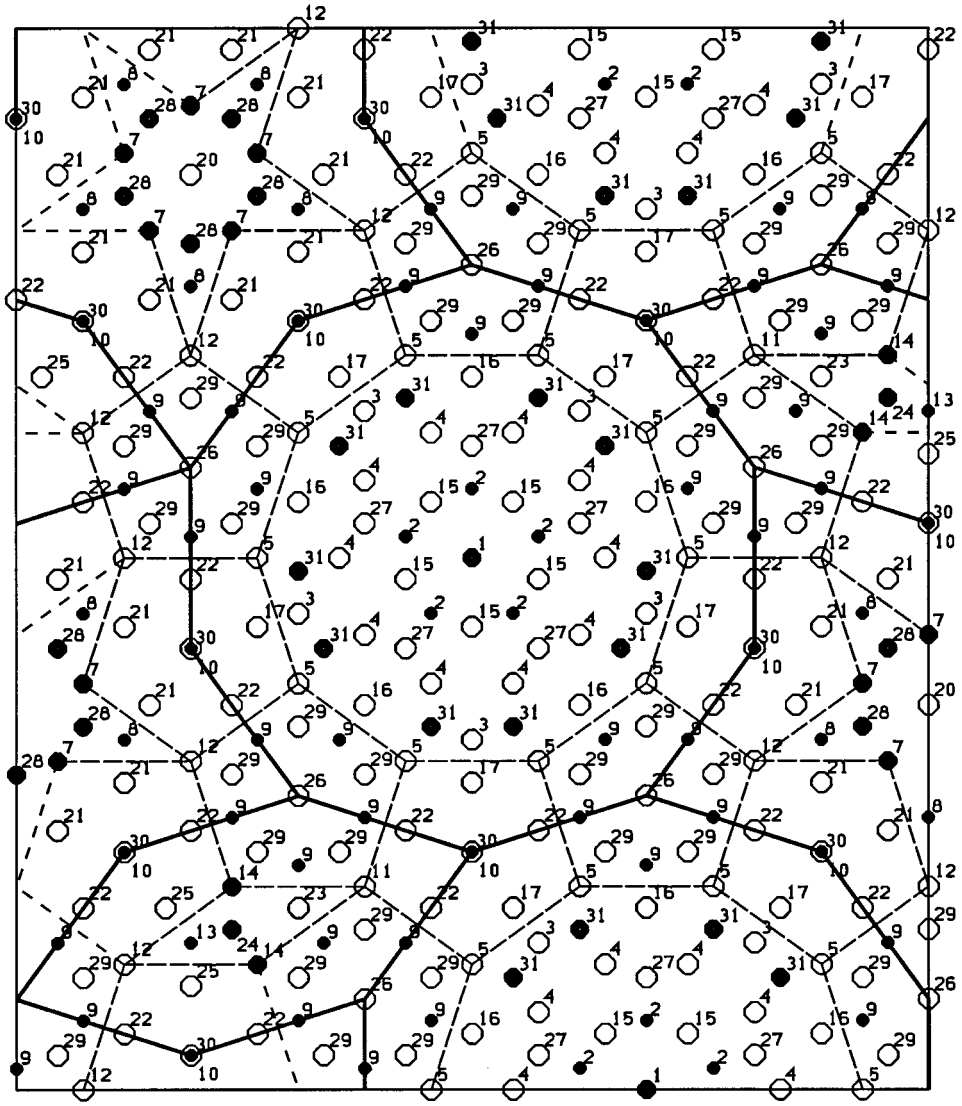

FIG. 8. Structural model for the τ^2-T phase: Projection of the positions of the atoms of half of the period (PFP planes) on a plane perpendicular to the periodic axis. Open circles represent Al atoms, large closed circles are the Pd atoms, small closed circles are the Mn atoms. The labels at each site indicate the toplogical type, cf. Fig. 6. Full lines show DPH tiling, dashed lines show decomposition of DPH tiling to small pentagonal columnar clusters.

The Pd band forms a broadband with maximum around ~ 4 eV below E_F. Pd atoms have almost the same size as Al atoms and they can replace Al atoms. The role of the third element is usually seen in the tuning of the position of the Fermi level relative to the local minimum in the total DOS. As the charge transfer to Pd atoms is small this effect is not too significant. It is interesting to observe the shallow depression in the Al-sp band just around the position of the maximum of Pd band. Its origin can be attributed to the hybridization between the Al-sp band and the Pd-d band.

D. Role of chemical constituents

We have attempted to examine the role of the different chemical constituents in the formation of the characteristic features of the DOS of the AlPdMn phases. Figure 7 shows the electronic structure of the τ^2-R phase with different chemical compositions. Figure 7(a) shows the total DOS of a model where all Al-Pd-Mn sites are occupied by Al atoms only; Fig. 7(b) represents the DOS of a phase where only the Pd atoms are replaced by Al atoms; Fig. 7(d) is the DOS of a phase with all transition metals replaced by Mn atoms. The system with Al atoms only is essentially free-electron like, with a weak structure-induced modulation of the shape of the DOS in the interval from -3 eV to 1 eV around E_F. The bandwidth is 11.3 eV. Figure 7(b) proves the important role of Mn atoms in the formation of the pseudogap in the partial Al-DOS around the Fermi level. The bandwidth is reduced to 10.2 eV. We assume that the pseudogap in the Al band is dominantly structure-induced. We note that the electron-ion matrix element which enters into the condition for creation of a pseudogap by the Hume-Rothery mechanism is small for the electron/atom (e/A) ratio of pure Al ($e/A=3$) and increases with decreasing e/A ratio. Most Al-based quasicrystals have almost the same bandwidth, around 10 eV, and the corresponding e/A ratio ranges from 2.0 to 2.4. The effect of the pseudogap in the DOS on the stability of the system is known and it seems that it is just the pseudogap in Al-DOS which significantly contributes to the stability of the whole system. The shape of the pseudogap is again a split double minimum. The origin of this feature is presumably in the sp-d hybridization between Al-sp band and Mn-d band. Replacement of further Al atoms by Pd has several effects on the Al-DOS; see Fig. 7(c): the DOS in the region around E_F clearly decreases and the missing states appear as a Pd

band in the region around -4 eV below E_F. The hybridization between the Al-sp and Pd-d bands creates a shallow depression in the Al band around the maximum of the Pd band. Eventually the bandwidth is further reduced by 0.3 eV which also possibly shifts the position of the Fermi level into the local minimum of the total DOS created by the coincidence of the positions of the local minima in the Al and Mn bands as discussed above. The effect of a replacement of all Pd atoms by Mn atoms is seen in Fig. 7(d). Due to the broadening of the Mn band the total DOS around E_F is strongly enhanced. The depression in the Al band disappears, otherwise the shape of the Al band remains intact. The bandwidth is further reduced to 9.7 eV.

E. Local environments and the local densities of states

It is also interesting to examine the local DOS at the topologically inequivalent sites. Figure 8 shows the projection of the PFP layers, i.e., the first half of the period of the model τ^2-T phase on the plane perpendicular to the the decagonal axis. Numbers at the atomic sites distinguish different topological sites. Only the types 10 and 30 are projected on the same place. The decoration of the second half of the period, i.e., of the pfp layers is analogous. It contains the same topological types. The exceptions are type 6 (located at inner corners of the pentagonal stars) which does not occur in the first half of the period, but occurs in the second one, and type 7, which does not occur in the second half of the period. The same holds for types 18, 19 and 20, 21. In the projection we see two types of small pentagonal clusters: one is centered by Al_{10} or with Mn_{30} and the other is centered by Al_{26}. We note that the decoration of both clusters in the second half of the period is just reversed. The assignment of chemical species to the topological sites was obtained by the optimization procedure described above.

Figure 9 represents the local densities of states for 31 topologically nonequivalent sites. Multiplicities (weights) of all sites are also indicated. The unit cell of the τ^2-T phase has 1058 sites. The greatest multiplicity belongs to Al_{29} (200 sites) and Al_{22} (104 sites). These atoms together with Al_{17} (40 sites) and Al_{21} (40 sites) are located in the rings of the small pentagonal clusters. They have well-resolved pseudogaps at the Fermi level indicating their significant contribution to the stability of the system. The deepest pseudogap appears on the Al_{10} (20 sites) which is situated in the center of half of the small pentagonal clusters. The remaining pentagonal clusters are centered by Al_{26} (40 sites), again with a rather deep local pseudogap. Manganese atoms from the rings forming small pentagonal clusters, Mn_9 (100 sites), and from the centers of these clusters, Mn_{30} (40 sites), have clearly visible bonding–antibonding splitting also contributing to the stability of the system. In the central region of the decagonal tile D we placed a decagonal ring of alternating Al_{15} and Mn_2 atoms. The local density of states of these Al atoms [Al_{15} (40 sites)] have again a pseudogap at the Fermi level due to interaction with Mn atoms. We note that Mn atoms in these positions are required also by stoichiometric consideration. From our optimization study we found that Pd atoms occupy predominantly sites in the regions outside of chains of small pentagons. From the local density of states of Pd_{31} (80 sites) we see that this position is

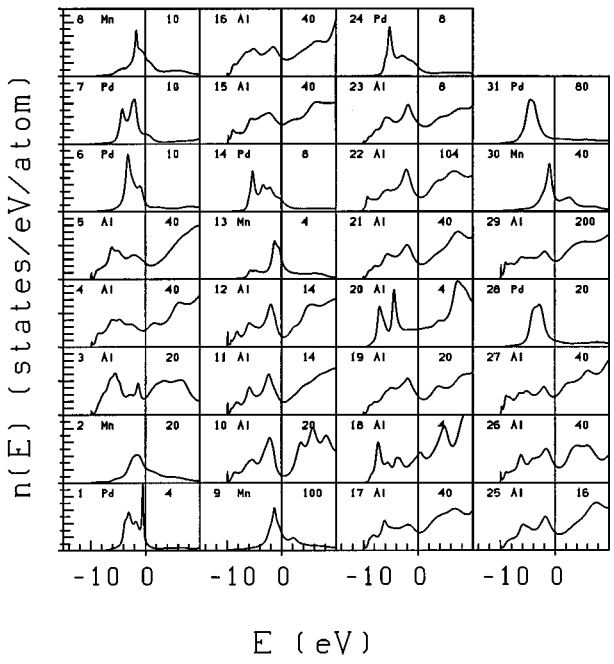

FIG. 9. Local densities of states of topologically different sites in the τ^2-T phase. The topological type is indicated in the upper left corner. Chemical type and multiplicity of the site are indicated, cf. Fig. 8. The range of the vertical scale is 1.0 states/eV/atom for Al atoms and 5.0 states/eV/atom for Pd and Mn atoms. Cf. text.

particularly suitable for palladium atoms. The same holds also for the sites Pd_{28} (20 sites) and Pd_6 (10 sites) and Pd_7 (10 sites) inside the pentagonal tiles P. By comparison the DOS of Pd_{28} is shifted to lower energies, possibly because of the interaction with the neighboring Mn_8 sites. Positions 6 and 7 could be occupied also by Al atoms. The proposal presented here is a consequence of stoichiometry considerations. The positions Pd_{14} (8 sites) and Pd_{24} (8 sites) inside the H tile are less favorable, but their relative weight is not too significant. From our calculations we found that the position in the center of the D tile is not proper for Mn atoms but we were not able to distinguish whether Al or Pd is here more suitable. The present Pd_1 (4 sites) occupation is again a result of stoichiometry considerations.

We note that decoration obtained by our optimization differs in some details from proposals of other authors. Beeli and Horiuchi[31] occupy position 1 by Mn, 2 by Pd, 3 by Mn, and 7, 28, and 31 by Al. In the model of Yamamoto[35] position 3 is occupied by TM, and 7 and 31 by Al. Position 4 (40 sites) in his model is vacant and he defines an additional position inside the D unit with the multiplicity 5.

F. Stability and the band-gap formation

The role of transition metals in Al-based Hume-Rothery alloys has been discussed in detail by Trambly de Laissardière *et al.*[14] As they pointed out, the essential mechanism for band-gap formation is, in addition to the effect of the diffraction of sp states by predominant Bragg planes, the influence of the transition-metal d states on sp states via sp-d coupling. In Sec. IV C we tried to estimate the importance of both contributions in the case of approximants to icosahedral

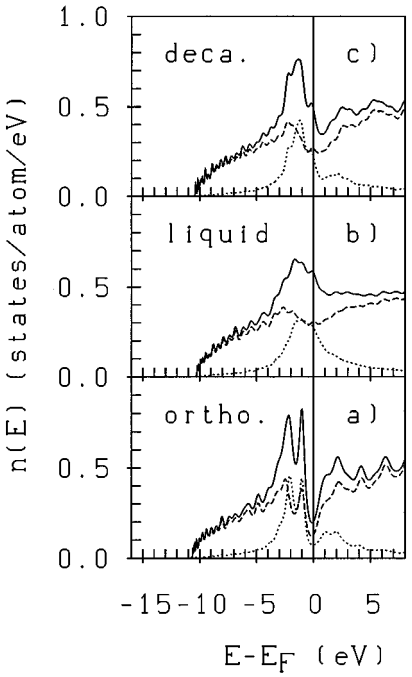

FIG. 10. Total and partial electronic densities of states of AlMn phases with different topological short-range order. (a) Crystalline orthorhombic Al_6Mn phase, (b) liquid phase at 1300 K with the same composition, (c) decagonal AlMn phase with almost the same composition $Al_{85.1}Mn_{14.9}$. Full line indicates total DOS, partial contributions to DOS: dashed line is for Al, dotted line is for Mn.

and decagonal quasicrystals. The crystalline Al_6Mn phase is a phase where the band-gap stabilization effect is particularly evident. The unit cell has *Cmcm* space-group symmetry (No. 63) and it contains 14 atoms per cell. Figure 10(a) represents the density of states for this phase. The structure-induced pseudogap in the Al band at E_F coincides with the hybridization pseudogap in the Mn-*d* band, resulting in a very deeep pseudogap in the total density of states. Figure 10(b) represents the density of states for the system with the same $Al_{85.7}Mn_{14.3}$ composition, but in a liquid state at 1300 K. The model was prepared by molecular-dynamics simulation using realistic Al-Mn interatomic potentials.[51] We see that a shallow structure-induced pseudogap at E_F in the Al band persists also in the liquid state. The Mn band has the character of an impurity band, broadened by positional disorder. Due to the disorder there is no definite phase relationship between Al-*sp* and Mn-*d* states, and hence no *sp*-*d* hybridization and further no pseudogap in the total DOS. Figure 10(c) is the density of states of the decagonal AlMn quasicrystal with the $Al_{85.1}Mn_{14.9}$ composition.

Figure 11 shows partial densities of states of Al atoms in different phases – T, R, and decagonal phase. The phases T and R differ mainly through a different alignment of the H tiles in the quasiperiodic plane. This leads also to a different topological arrangement of Hiraga's pentagonal columnar clusters. The effect of this rearrangement on the shape of the pseudogap around E_F is evident. The characteristic split double minimum in the Al-DOS which exists in any larger approximant to the decagaonal phase can be interpreted as R-like arrangements of the structural units.

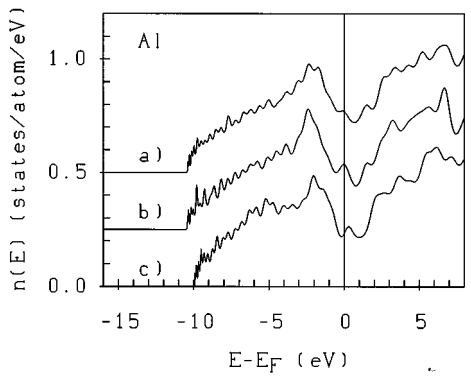

FIG. 11. Partial electronic densities of states of Al atoms in different phases. Influence of topological arrangement of pentagonal columnar clusters on the shape of pseudogap around E_F. (a) Al-DOS in the T phase, (b) Al-DOS in the R phase, (c) Al-DOS in the decagonal phase.

The influence of diffraction of the Al *sp* states by pseudo-Bragg planes in a decagonal quasicrystal is seen in Fig. 12. It represents dispersion relations derived from the positions of the maxima in the Bloch-spectral function $F(\mathbf{k},E)$, i.e., a density of states projected onto a plane wave with a **k** vector in the quasiperiodic plane propagating along a twofold symmetry axis, cf. Fig. 3. The projection is on Al states only. At low energy we can clearly observe propagating states with parabolic dispersion relation around **k** vectors corresponding to the strong diffraction peaks. These diffraction peaks correspond to the Γ points of the 5D reciprocal lattice projected onto the 3D physical space.[52,53] At higher energies the propagating modes merge with many dispersionless bands. We also observe that the paraboliclike states originating from **k** vectors 0 and 26 (in units 2π/a) intersect at energy $E\sim1.0$ eV below E_F. Another pair of dominant free-electron pa-

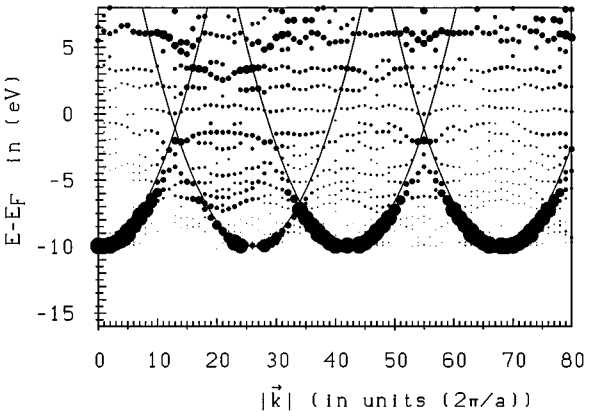

FIG. 12. Dispersion relations derived from the positions of maxima of the spectral function $F(\mathbf{k},E)$ of the τ^2-T approximant to the decagonal AlPdMn phase, calculated as a projection of the Al-DOS onto a plane wave with a wave vector **k** vector oriented along a twofold axis in the quasiperiodic plane, cf. Fig. 3. Propagating states with parabolic dispersion around **k** points corresponding to strong diffraction peaks at $|\mathbf{k}|=0$, 26, 42, and 68 in units of ($2\pi/a$) (where a is the lattice constant) are emphasized by full lines. Free-electron parabolas (full lines) corresponding to pairs of strong diffraction peaks intersect close to the Fermi level.

rabolas issuing from **k** vectors 42 and 68 (in units $2\pi/a$) crossects at the same energy. The strong Γ points form a Fibonacci sequence along the twofold symmetry axis in the quasiperiodic plane. The distance 26 (in units $2\pi/a$) between the strong Γ points corresponds to the longer element of the Fibonacci sequence. The same Fibonacci sequence of strong Γ points exists along any tenfold symmetry axis in the quasiperiodic plane. The intersections of the free-electron parabolas is the dominant factor in the formation of a Hume-Rothery-like pseudogap in DOS.

V. DISCUSSION AND SUMMARY

We have performed first-principles calculations of the electronic structure of large approximants to decagonal AlPdMn quasicrystals and related crystalline structures (R, T, τ^2-R, and τ^2-T phases). These results supplement our earlier investigations of a hierarchy of approximants to icosahedral Al-Pd-Mn quasicrystals. For the icosahedral phases we had found that the 2/1 and all higher-order approximants (but not the hypothetical 1/1 approximant) profit from an appreciable band-gap stabilization through the formation of a deep DOS minimum at the Fermi level. We had also pointed out that the strength of the pseudogap depends not only on the electron-lattice interaction, but also in the hybridization of the Al-s,p states forming the pseudogap with Mn-d states. This hybridization leads to an enhancement of the Al-pseudopotential matrix elements as shown some time ago by Heine[54] and as recently discussed for the special case of the formation of Hume-Rothery pseudogaps in Al−transition-metal alloys by Trambly de Laissardière *et al.*[14]

In the present paper we show that a structure-induced pseudogap in the Al band exists also in the decagonal Al-Pd-Mn and its approximant phases. Again we have found evidence for the important role of the sp-d hybridization in the formation of the pseudogap. However there are two important differences between the decagonal and icosahedral phases: (a) due to the higher Mn content, the broadened Mn band overlaps with the Fermi level. This leads to a relatively high DOS at E_F. (b) The effect of sp-d hybridization in formation of the shape of the pseudogap is more visible. The DOS minimum in the Al band is clearly split into two subminima which coincide with similar features in Mn-band. We have shown that this characteristic feature is clearly related to the existence of local arrangements of the structural units such as they are found in the R phase. (c) The Fermi level is pinned in the first subminimum of the total DOS, contrary to the case of the icosahedral phase where the Fermi level is located in the second, deeper subminimum.

If we compare the crystalline and quasicrystalline phases, we find that the importance of the Hume-Rothery-like band-gap stabilization decreases in the sequence crystalline (Al_6Mn)—icosahedral ($Al_{70}Pd_{22}Mn_8$)—decagonal ($Al_{70}Pd_{13}Mn_{17}$) phases.

In icosahedral AlPdMn we could not identify any independent structural unit with increased stability.[15] The basic structural motif consists of large interpenetrating icosahedral clusters whose size may be extended to infinity by inflation. In decagonal AlPdMn phases such a unit has been identified by Hiraga and Sun.[22] It is a small pentagonal columnar cluster which seems to be a basic structural constituent of all discussed phases.

The DPH tiling observed in HREM images of AlPdMn phases can be obtained as a result of maximal-density packing of unit disks with the condition that the centers of the disks are constrained to a subset of vertices of a binary tiling.[39] Decagons (D tiles) and pentagonal stars (P tiles) are here identified with the unit disks. We can formulate also a complementary opinion to the origin of the decagonal order based on the tiling of Hiraga's small pentagonal clusters. Chains of relatively stable pentagonal clusters form stable crystalline phases (T or R phase). In this case the packing of the small pentagonal tiles is densest, leaving open only small rhombi inside the H tiles. Disordering this densest structure opens pentagonal and decagonals regions inside P and D tiles, respectively, which are filled preferably by Pd atoms. This regions can be considered as palladium-rich bubbles in the network formed by chains of small pentagonal clusters. It seems that the decagonal order in the plane is induced predominantly by geometrical constraints for the packing of pentagons in a plane—in a similar way the densest packing of disks in a plane induces hexagonal symmetry. However, this may be only partially true, as in the densest packing of Hiraga's small pentagonal clusters these clusters would fill also the region inside the D tiles. Therefore the D tile should also have certain relative stability supported presumably by the central region of the tile occupied mostly by Al and Mn atoms. The role of Pd atoms can be seen rather negatively than positively in contribution to the stability. This view is also supported by the fact that the τ^2-R phase, which contains a smaller fraction of D and P units per cell (0.33 for each tile), is more stable than the τ^3-T phase containing fractions of 0.42 and 0.36 of D and P tiles per unit cell, respectively. For the stabilization of the decagonal phase is therefore also important to consider the entropy term in the free energy. This conclusion is in agreement with the experimental observation that the decagonal AlPdMn phase exists only as a high-temperature phase.[22]

ACKNOWLEDGEMENT

This work has been supported by the Jubiläumsfonds der Österreichischen Nationalbank under Project No. P5658.

*Permanent address: Institute of Physics, Slovak Academy of Sciences, SK 84228 Bratislava, Slovakia.

[1] For reviews see, e.g., *Quasicrystals—The State of the Art* , edited by D. P. DiVincenzo and P. J. Steinhardt (World Scientific, Singapore, 1991); *Quasicrystals*, edited by T. Fujiwara and T. Ogawa (Springer, Berlin, 1990); C. Janot, *Quasicrystals—A Primer* (Oxford University Press, Oxford, 1992).

[2] A. P. Smith and N. W. Ashcroft, Phys. Rev. Lett. **59**, 1356 (1987).

[3] J. Friedel and F. Denoyer, C. R. Acad. Sci. **305**, 171 (1987).

[4] W. Hume-Rothery, J. Inst. Met. **35**, 295 (1926); W. Hume-Rothery and G. V. Raynor, *The Structure of Metals and Alloys* (The Institute of Metals, London, 1954).

[5] H. Jones, Proc. Phys. Soc. **49**, 250 (1937).

[6] T. Fujiwara, Phys. Rev. B **40**, 942 (1989).
[7] T. Fujiwara and T. Yokokawa, Phys. Rev. Lett. **66**, 333 (1991).
[8] T. Fujiwara, J. Non-Cryst. Solids **156-158**, 865 (1993).
[9] J. Hafner and M. Krajčí, Phys. Rev. Lett. **68**, 2321 (1992); Phys. Rev. B **47**, 11 795 (1993).
[10] M. Windisch, M. Krajčí, and J. Hafner, J. Phys. Condens. Matter **6**, 6977 (1994).
[11] M. Krajčí and J. Hafner, Europhys. Lett. **27**, 147 (1994).
[12] J. Friedel, Helv. Phys. Acta **61**, 538 (1988).
[13] J. Friedel, Philos. Mag. B **65**, 1125 (1992).
[14] G. Trambly de Laissardière, D. Nguyen Manh, L. Maguad, J. P. Julien, F. Cyrot-Lackmann, and D. Mayou, Phys. Rev. B **52**, 7920 (1995).
[15] M. Krajčí. M. Windisch, J. Hafner, G. Kresse, and M. Mihalkovič, Phys. Rev. B **51**, 17 355 (1995).
[16] G. Trambly de Laissardière and T. Fujiwara, Phys. Rev. B **50**, 9843 (1994).
[17] S. E. Burkov, Phys. Rev. Lett. **67**, 614 (1991).
[18] Z. M. Stadnik, G. W. Zhang, A. P. Tsai, and A. Inoue, Phys. Lett. A **198**, 237 (1995); Phys. Rev. B **51**, 11 358 (1995).
[19] R. F. Sabiryanov, S. K. Bose, and S. E. Burkov, J. Phys. Condens. Matter **7**, 5437 (1995).
[20] P. Kramer, A. Quandt, M. Schlottmann, and T. Schneider, Phys. Rev. B **51**, 8815 (1995).
[21] C. Beeli, H. U. Nissen, and J. Robadey, Philos. Mag. Lett **63**, 87 (1991).
[22] K. Hiraga and W. Sun, Philos. Mag. Lett. **67**, 117 (1993).
[23] M. Audier, M. Durand-Charre, and M. de Boissieu, Philos. Mag. B **68**, 607 (1993).
[24] O. K. Andersen, D. Jepsen, and M. Šob, in *Electronic Band Structure and its Applications*, edited by M. Youssouff (Springer, Berlin, 1987).
[25] S. K. Bose, S. S. Jaswal, O. K. Andersen, and J. Hafner, Phys. Rev. B **37**, 9955 (1988).
[26] T. Gödecke and R. Lück, Z. Metallkd. **86**, 109 (1995); T. Gödecke, R. Lück, and C. Beeli, in *Proceedings of the 5th International Conference on Quasicrystals*, edited by C. Janot and R. Mosseri (World Scientific, Singapore, 1995), p. 644.
[27] K. Hiraga, M. Kaneko, Y. Matsuo, and S. Hashimoto, Philos. Mag. B **67**, 193 (1993).
[28] M. A. Taylor, Acta Crystallogr. **14**, 84 (1961).
[29] K. Robinson, Acta Crystallogr. **7**, 494 (1954).
[30] P. Villars and L. D. Calvet, *Pearson's Handbook of Crystallographic Data for Intermetallic Phase* (American Society for Metals, Material Park, OH, 1991), Vol. 1.
[31] C. Beeli and S. Horiuchi, Philos. Mag. B **70**, 215 (1994).
[32] A. Waseda, H. Morioka, K. Kimura, and H. Ino, Philos. Mag. Lett. **65**, 25 (1992).
[33] A. D. I. Nicol, Acta Crystallogr. **9**, 285 (1953).
[34] W. Steurer, T. Haibach, B. Zhang, C. Beeli, and H. U. Nissen, J. Phys. Condens. Matter **6**, 613 (1994).
[35] A. Yamamoto, Y. Matsuo, T. Yamanoi, A. P. Tsai, K. Hiraga, and T. Masumoto, in *Proceedings of the International Conference on Aperiodic Crystals*, edited by G. Chapuis and W. Paciorek (World Scientific, Singapore 1994), p. 393.
[36] M. Duneau and M. Audier, in *Lectures on Quasicrystals*, edited by F. Hippert and D. Gratias (Les Editions de Physique, Les Ulis, France 1995), p. 283.
[37] K. Hiraga, in *Proceedings of the International Conference on Aperiodic Crystals* (Ref. 35) p. 341.
[38] E. Cockayne, Phys. Rev. B **51**, 14 958 (1995).
[39] M. Mihalkovič, in *Proceedings of the International Conference on Aperiodic Crystals* (Ref. 35) p. 552.
[40] C. Beeli, P. Stadelmann, R. Lück, and T. Gödecke, in *Proceedings of the International Conference on Aperiodic Crystals*, (Ref. 35), p. 361.
[41] K. Hiraga, J. Non-Cryst. Solids **153**, 30 (1993).
[42] P. Oelhafen, in *Glassy Metals II*, edited by H. Beck and H. J. Güntherodt (Springer, Berlin, 1983), p. 283.
[43] W. Jank, C. Hausleitner, and J. Hafner, Europhys. Lett. **16**, 473 (1991).
[44] C. Hausleitner, M. Tegze, and J. Hafner, J. Phys. Condens. Matter **4**, 9557 (1992).
[45] V. Heine, D. Bullett, R. Haydock, and M. J. Kelly, in *Solid State Physics: Advances in Research and Applications*, edited by H. Ehrenreich, D. Turnbull, and F. Seitz (Academic, New York, 1980), Vol. 35.
[46] M. U. Lucchini and C. M. M. Nex, J. Phys. C **20**, 3125 (1987).
[47] C. M. M. Nex, J. Phys. A **11**, 653 (1978).
[48] U. von Barth and L. Hedin, J. Phys. C **4**, 2064 (1972).
[49] J. Hafner and M. Krajčí, Phys. Rev. B **47**, 1084 (1993); J. Phys. Condens. Matter **5**, 2489 (1993).
[50] O. K. Andersen, in *Electrons at the Fermi Surface*, edited by M. Springford (Cambridge University Press, London, 1980).
[51] R. Phillips and M. Widom, J. Non-Cryst. Solids **153-154**, 416 (1993).
[52] K. Niizeki, J. Phys. A **22**, 4295 (1989).
[53] K. Niizeki and T. Akamatsu, J. Phys. Condens. Matter **2**, 2759 (1989).
[54] V. Heine, in *The Physics of Metals*, edited by J. M. Ziman (Cambridge University Press, Cambridge, 1968), Vol. 1, p. 1.